Institute of Computer Science
Academy of Sciences of the Czech Republic

Numerical Analysis of the Long Bone with the Marrow

Luboš Tomášek, Josef Daněk

Technical report No. 1013

December 3, 2007

Abstract:

The report deals with the mathematical and numerical analysis of a loaded human tibia filled by the marrow tissue. The stress distribution in the marrow is focused. Two different rheological approaches were chosen. The elastic and viscoplastic models are formulated and shortly discussed. The numerical results refer to the elastic case with Coulomb's law of friction.

Keywords:
mathematical modelling, variational formulation, contact problems, elasticity, viscoplasticity, Bingham fluid, tibia

1 Introduction

This part of grant deals with the modelling of loaded human tibia. Particularly, we are interested in the stress propagation in the marrow tissue when certain mechanical loading is applied to tibia. The motivation for this research comes from the area of development of artifical devices. Such devices are designed for replacing disturbed parts of human skeleton. This contribution might help in future to estimate the influence of an artificial device, e.g. artificial knee joint, on the marrow.

Firstly, the mathematical formulations are provided. We consider the elastic and the viscoplastic approaches. The analysis of the viscoplastic case is presented to obtain some kind of solution existence result. Eventually, the numerical results of the elastic case are provided.

2 The elastic problem definition

2.1 Classical formulation

Let $\Omega \subset \mathbb{R}^d$ ($d \in \{2;3\}$) be a bounded domain with Lipschitz boundary $\partial\Omega$. Let $\partial\Omega = \Gamma_D \cup \Gamma_L$, $\Gamma_D \cap \Gamma_L = \emptyset$ and $\mu_{d-1}(\Gamma_D) > 0$. Let $\Omega = \Omega^k \cup \Omega^l$, $\Omega^k \cap \Omega^l = \emptyset$. $\Gamma_C = \partial\Omega^k \cap \partial\Omega^l$ denotes the area where the contact condition between the bodies takes place. Unknown $\mathbf{u} : \Omega \to \mathbb{R}^d$ represents the displacement. Given vectors $\mathbf{f} : \Omega \to \mathbb{R}^d$ and $\mathbf{u}_0 : \Gamma_D \to \mathbb{R}^d$ stand for the volume forces and the Dirichlet boundary condition, respectively. Standard Hookean law applies, i.e. the symmetric stress tensor $\mathbf{T} : \Omega \to \mathbb{R}^{d\times d}$ ($\mathbf{T} = \{\tau_{ij}\}_{i,j=1}^d$) is expressed by

$$\mathbf{T} = \mathbf{T}(\mathbf{u}) = \mathbb{C}_{ijkl}\, \mathbf{e}_{kl}(\mathbf{u}),$$

where $\mathbf{e} = \frac{1}{2}(\nabla\mathbf{u} + (\nabla\mathbf{u})^T)$ and $\mathbb{C}$ is the elastic coefficient tensor. Furthermore, we specify boundary condition $\mathbf{P} : \Gamma_L \to \mathbb{R}^d$ representing the loading forces. An unit outward normal vector is indicated by $\mathbf{n}$. u_n^j stands for normal component of $\mathbf{u}$ on Γ_C belonging to Ω^j. $\mathcal{F}_c^{kl}$ are the coefficients of friction, τ_t the tangential stress force and $\mathbf{u}_t^j$ the tangential displacement on Γ_C belonging to Ω^j. We're interested in the following problem.

Problem 2.1 *Find* $\mathbf{u} \in (\mathbf{C}^2(\Omega))^d$ *such that*

$$\begin{aligned}
-\operatorname{div}\mathbf{T} &= \mathbf{f} \quad \text{in } \Omega, && (1)\\
\mathbf{u} &= \mathbf{u}_0 \quad \text{on } \Gamma_D, && (2)\\
\mathbf{T}\,\mathbf{n} &= \mathbf{P} \quad \text{on } \Gamma_L, && (3)\\
u_n^k - u_n^l &= 0 \quad \text{on } \Gamma_C, && (4)\\
|\tau_t| &\le \mathcal{F}_c^{kl}\,|\tau_n| \quad \text{on } \Gamma_C, && (5)\\
|\tau_t| < \mathcal{F}_c^{kl}\,|\tau_n| &\Rightarrow \mathbf{u}_t^k - \mathbf{u}_t^l = 0 \quad \text{on } \Gamma_C, && (6)\\
|\tau_t| = \mathcal{F}_c^{kl}\,|\tau_n| &\Rightarrow \exists\,\lambda \ge 0, \quad \mathbf{u}_t^k - \mathbf{u}_t^l = -\lambda\tau_t \quad \text{on } \Gamma_C. && (7)
\end{aligned}$$

2.2 Variational formulation

Let us introduce $\mathbf{W} = [H^1(\Omega)]^d$, $\|\mathbf{v}\|_{\mathbf{W}} = (\sum_{i\le d}\|\mathbf{v}_i\|_{1,\Omega}^2)^{\frac{1}{2}}$ and the sets of virtual and admissible displacements $\mathbf{V}_0 = \{\mathbf{v} \in \mathbf{W} \mid \mathbf{v} = \mathbf{0} \text{ on } \Gamma_D\}$, $\mathbf{V} = \mathbf{u}_0 + \mathbf{V}_0$, $K = \{\mathbf{v} \in \mathbf{V} \mid v_n^k - v_n^l = 0 \text{ on } \Gamma_C\}$. Assume that $u_{0n}^k - u_{0n}^l = 0$ on Γ_C. Let $\mathbb{C}_{ijkl} \in L^\infty(\Omega)$, $F_i \in L^2(\Omega)$, $P_i \in L^2(\Gamma_L)$, $\mathbf{u}_0 \in [H^1(\Omega)]^d$. Then we have to solve the following variational problem:

Problem 2.2 *Find a function* $\mathbf{u}$, $\mathbf{u} - \mathbf{u}_0 \in K$, *such that*

$$a(\mathbf{u}, \mathbf{v} - \mathbf{u}) + j(\mathbf{v}) - j(\mathbf{u}) \ge L(\mathbf{v} - \mathbf{u}) \qquad \forall\,\mathbf{v} \in K \tag{8}$$

holds, where

$$\begin{aligned}
a(\mathbf{u}, \mathbf{v}) &= \textstyle\int_\Omega \mathbb{C}_{ijkl}\mathbf{e}_{ij}(\mathbf{u})\mathbf{e}_{kl}(\mathbf{v})\,\mathrm{d}x,\\
j(\mathbf{v}) &= \textstyle\int_{\Gamma_C} \mathcal{F}_c^{kl}|\tau_n| \mid \mathbf{v}_t^k - \mathbf{v}_t^k \mid \mathrm{d}S,\\
L(\mathbf{v}) &= \textstyle\int_\Omega F_i v_i\,\mathrm{d}x - \int_{\Gamma_L} P_i v_i\,\mathrm{d}S.
\end{aligned} \tag{9}$$

The analysis of the problem and the existence results can be found in [3].

3 The viscoplastic problem definition and analysis

3.1 Classical formulation

Let $\Omega \subset \mathbb{R}^d$ ($d \in \{2;3\}$) be a bounded domain with Lipschitz boundary $\partial\Omega$. Let $\partial\Omega = \Gamma_D \cup \Gamma_L$, $\Gamma_D \cap \Gamma_L = \emptyset$ and $\mu_{d-1}(\Gamma_D) > 0$. The unknown $\mathbf{v} : \Omega \to \mathbb{R}^d$ denotes velocity. The given vector $\mathbf{f} : \Omega \to \mathbb{R}^d$ stands for the volume forces. The dependence of the symmetric stress tensor $\mathbf{T} : \Omega \to \mathbb{R}^{d\times d}$ ($\mathbf{T} = \{\tau_{ij}\}_{i,j=1}^d$) on velocity $\mathbf{v}$ will be investigated later. Furthermore, we specify boundary condition $\mathbf{P} : \Gamma_L \to \mathbb{R}^d$ representing the loading forces. An unit outward normal vector is indicated by $\mathbf{n}$. We're interested in the analysis of the following problem.

Problem 3.1 *Find* $\mathbf{v} \in (\mathbf{C}^2(\Omega))^d$ *such that*

$$\begin{aligned} \operatorname{div}\mathbf{v} &= 0 \quad \text{in } \Omega, && (10)\\ -\operatorname{div}\mathbf{T} &= \mathbf{f} \quad \text{in } \Omega, && (11)\\ \mathbf{v} &= \mathbf{0} \quad \text{on } \Gamma_D, && (12)\\ \mathbf{T}\,\mathbf{n} &= \mathbf{P} \quad \text{on } \Gamma_L. && (13) \end{aligned}$$

Any solution of Problem 3.1 is called a *classical solution* in this section. In order to couple the equations (10) and (11) and to formulate the constitutive relations, we need to specify the dependence of the stress tensor $\mathbf{T}$ on the velocity $\mathbf{v}$ in Problem 3.1.

Let's assume that the stress tensor $\mathbf{T}$ can be decomposed into the spherical and the deviatoric part, denoted by $\mathbf{T}^\delta$,

$$\mathbf{T} = -p\,\mathbf{I} + \mathbf{T}^\delta. \tag{14}$$

Here, $p : \Omega \to \mathbb{R}$ has the meaning of the pressure.

The rheology of the Bingham fluid is described by the relations[1]

$$|\mathbf{T}^\delta| \le g \quad \Rightarrow \quad \mathbf{D} = \mathbf{0}, \tag{15}$$

$$|\mathbf{T}^\delta| > g \quad \Rightarrow \quad \mathbf{D} \neq \mathbf{0} \quad \wedge \quad \mathbf{T}^\delta = g\,\frac{\mathbf{D}}{|\mathbf{D}|} + \nu\,\mathbf{D}, \tag{16}$$

where $\mathbf{D} := \mathbf{D}(\mathbf{v}) = \frac{1}{2}(\nabla\mathbf{v} + (\nabla\mathbf{v})^T)$. The non-negative material constant g represents the threshold of plasticity ($[g] = m^2\,s^{-2}$) and the positive material constant ν the kinematic viscosity ($[\nu] = m^2\,s^{-1}$). The case $g = 0$ results in an ordinary Newtonian fluid. If $g \to \infty$, the material behaves like a rigid body. Moreover, both implications (15) and (16) can be trivially extended to equivalences.

The deviator $\mathbf{S}^\delta$ of a general tensor $\mathbf{S}$ is defined by $\mathbf{S}^\delta_{ij} := \mathbf{S}_{ij} - \frac{1}{d}\mathbf{S}_{kk}\delta_{ij}$. For the case $|\mathbf{T}^\delta| > g$, using the incompressibility equation (10), this means that the deviator of $\mathbf{T}$ is equal to $\mathbf{T}^\delta$ defined in (16), so that the notation introduced in (14) is clarified.

To derive the inverse constitutive relation for the case $|\mathbf{T}^\delta| > g$ we manage with (16).

$$\mathbf{D} = \frac{|\mathbf{D}|}{g + \nu\,|\mathbf{D}|}\mathbf{T}^\delta = \frac{|\mathbf{D}|}{|\mathbf{T}^\delta|}\mathbf{T}^\delta. \tag{17}$$

Again, from (16) and from (17) it follows

$$\begin{aligned} \mathbf{T}^\delta &= g\,\frac{\mathbf{T}^\delta}{|\mathbf{T}^\delta|} + \nu\,\mathbf{D}, && (18)\\ \mathbf{D} &= \frac{1}{\nu}\Big(1 - \frac{g}{|\mathbf{T}^\delta|}\Big)\mathbf{T}^\delta. && (19) \end{aligned}$$

[1] $|\mathbf{S}|^2 := \mathbf{S}\cdot\mathbf{S}$, $\mathbf{S}\cdot\mathbf{T} = \mathbf{S}_{ij}\mathbf{T}_{ij}$, assuming Einstein summation convention throughout the document.

3.2 Weak formulation

We now derive the weak formulation of Problem 3.1. Let's define the space $\mathbf{V}$ by

$$\mathbf{V} = \{\mathbf{v} \in (\mathbf{W}^{1,2}(\Omega))^d;\ \mathbf{v} = 0 \text{ on } \Gamma_D,\ \operatorname{div}\mathbf{v} = 0 \text{ in } \Omega\}.$$

Assume that $\mathbf{v}$ is a classical solution of Problem 3.1, $\mathbf{f}$ and $\mathbf{P}$ are seemly chosen to ensure the existence of all integrals and $\mathbf{w} \in \mathbf{V}$. When we multiply equation (11) by $\mathbf{w} - \mathbf{v}$, integrate over Ω, use Green's theorem, incompressibility condition (10), symmetry of $\mathbf{T}$ and boundary conditions (12), (13), we obtain

$$\int_\Omega \mathbf{T}^\delta \cdot \mathbf{D}(\mathbf{w} - \mathbf{v})\,\mathrm{d}x = \underbrace{\int_\Omega \mathbf{f}_i(\mathbf{w}_i - \mathbf{v}_i)\,\mathrm{d}x}_{=:(\mathbf{f},\mathbf{w}-\mathbf{v})} + \underbrace{\int_{\Gamma_L} \mathbf{P}_i(\mathbf{w}_i - \mathbf{v}_i)\,\mathrm{d}S}_{=:(\mathbf{P},\mathbf{w}-\mathbf{v})}. \tag{20}$$

Left hand side of (20) can be decomposed to

$$\int_\Omega \mathbf{T}^\delta \cdot \mathbf{D}(\mathbf{w} - \mathbf{v})\mathrm{d}x = \int_{\Omega_r} \mathbf{T}^\delta \cdot \mathbf{D}(\mathbf{w} - \mathbf{v})\mathrm{d}x \ + \int_{\Omega_f} \mathbf{T}^\delta \cdot \mathbf{D}(\mathbf{w} - \mathbf{v})\mathrm{d}x, \tag{21}$$

where $\Omega_r = \Omega \cap \{|\mathbf{D}| = 0\}$, $\Omega_f = \Omega \cap \{|\mathbf{D}| > 0\}$. Applying (15), (16) gives

$$\int_{\Omega_r} \mathbf{T}^\delta \cdot \mathbf{D}(\mathbf{w} - \mathbf{v})\mathrm{d}x \le \int_{\Omega_r} |\mathbf{T}^\delta|\,|\mathbf{D}(\mathbf{w})|\mathrm{d}x \le \int_{\Omega_r} g\,|\mathbf{D}(\mathbf{w})|\mathrm{d}x, \tag{22}$$

$$\int_{\Omega_f} \mathbf{T}^\delta \cdot \mathbf{D}(\mathbf{w} - \mathbf{v})\mathrm{d}x = \int_{\Omega_f} \frac{g}{|\mathbf{D}|}\mathbf{D} \cdot \mathbf{D}(\mathbf{w} - \mathbf{v})\mathrm{d}x + \int_{\Omega_f} \nu\,\mathbf{D} \cdot \mathbf{D}(\mathbf{w} - \mathbf{v})\mathrm{d}x, \tag{23}$$

$$\int_{\Omega_f} \frac{g}{|\mathbf{D}|}\mathbf{D} \cdot \mathbf{D}(\mathbf{w} - \mathbf{v})\mathrm{d}x \le \int_{\Omega_f} g\,|\mathbf{D}(\mathbf{w})|\mathrm{d}x - \int_{\Omega_f} g\,|\mathbf{D}|\mathrm{d}x. \tag{24}$$

Putting the above equations and inequalities together, we have

$$\int_\Omega \nu\,\mathbf{D} \cdot \mathbf{D}(\mathbf{w} - \mathbf{v})\mathrm{d}x + j(\mathbf{w}) - j(\mathbf{v}) \ge (\mathbf{f}, \mathbf{w} - \mathbf{v}) + (\mathbf{P}, \mathbf{w} - \mathbf{v}), \tag{25}$$

where $j(\mathbf{u}) = \int_\Omega g\,|\mathbf{D}(\mathbf{u})|\mathrm{d}x$, for any $\mathbf{u} \in \mathbf{V}$. The weak formulation follows immediately.

Problem 3.2 *Find* $\mathbf{v} \in \mathbf{V}$ *such that (25) holds for all* $\mathbf{w} \in \mathbf{V}$.

Any solution of Problem 3.2 is called a *weak solution* in this section. It is now obvious that any classical solution is also a weak solution. To sketch the proof of the reverse implication, we limit ourselves to the case $\Omega_f = \Omega$. The variation of j defined by

$$j'(\mathbf{v}, \mathbf{w}) = \lim_{h \to 0} \frac{1}{h}(j(\mathbf{v} + h\mathbf{w}) - j(\mathbf{v})) \tag{26}$$

is equal to

$$j'(\mathbf{v}, \mathbf{w}) = \int_{\Omega_f} g\frac{\mathbf{D} \cdot \mathbf{D}(\mathbf{w})}{|\mathbf{D}|}\mathrm{d}x. \tag{27}$$

Setting $w := v \pm \lambda\bar{w}, \lambda > 0$ in (25) and limit passage $\lambda \to 0+$ gives

$$\int_\Omega \nu\,\mathbf{D} \cdot \mathbf{D}(\mathbf{w})\mathrm{d}x + j'(\mathbf{v}, \mathbf{w}) = (\mathbf{f}, \mathbf{w}) + (\mathbf{P}, \mathbf{w}). \tag{28}$$

When we now apply Green's theorem, consider (27), (10) and boundary conditions (12) and (13), (28) can be rewritten to

$$\int_\Omega (\operatorname{div}\mathbf{T} + \mathbf{f}) \cdot \mathbf{w}\,\mathrm{d}x = 0. \tag{29}$$

Using the representation theorem on Hilbert space $\mathbf{V}$ implies the equality (11) in $\mathbf{V}^\star$.

3.3 Variational formulation

We're now going to set up the variational formulation of Problem 3.2, prove the existence of a variational solution and show the equivalence of weak and variational solutions.

Let's define functional $J : \mathbf{V} \to \mathbf{R}$ by

$$J(\mathbf{w}) := \int_\Omega \frac{1}{2}\,\nu\,|\mathbf{D}(\mathbf{w})|^2\,\mathrm{d}x + j(\mathbf{w}) - (\mathbf{f},\mathbf{w}) - (\mathbf{P},\mathbf{w}). \tag{30}$$

Problem 3.3 *Find* $\mathbf{v} \in \mathbf{V}$ *such that* $J(\mathbf{v}) \le J(\mathbf{w})\ \forall\,\mathbf{w} \in \mathbf{V}$.

Any solution of Problem 3.3 is called a *variational solution* in this section.

The existence of a variational solution can be proved by *direct method*. The functional J is weakly coercive, i.e. $J(\mathbf{w}) \to +\infty$ as $\|\mathbf{w}\| \to \infty$. Let's take a (minimizing) sequence $\{\mathbf{w}_k\}_{k=1}^{\infty}$ fulfilling $J(\mathbf{w}_k) \to \inf_{\mathbf{w}\in\mathbf{V}} J(\mathbf{w})$. Such a sequence has to be bounded thanks to the weak coercivity of J. Since $\mathbf{V}$ is reflexive, there exists $\mathbf{v} \in \mathbf{V}$ such that $\mathbf{w}_k \rightharpoonup \mathbf{v}$ in $\mathbf{V}$. J is also lower semicontinuous and convex which implies J weakly lower semicontinuous (see [5]). The chain of (in)equalities

$$J(\mathbf{v}) \le \liminf_{k\to\infty} J(\mathbf{w}_k) = \lim_{k\to\infty} J(\mathbf{w}_k) = \inf_{\mathbf{w}\in\mathbf{V}} J(\mathbf{w}) \tag{31}$$

proves that the weak limit $\mathbf{v} \in \mathbf{V}$ is the solution of Problem 3.3.

Setting $\mathcal{H}(\mathbf{w}) = \int_\Omega \frac{1}{2}\,\nu\,|\mathbf{D}(\mathbf{w})|^2\,\mathrm{d}x - (\mathbf{f},\mathbf{w}) - (\mathbf{P},\mathbf{w})$, $\mathcal{I}(\mathbf{w}) = j(\mathbf{w})$ in Lemma 3.1 shows the equivalence of weak and variational solution.

Lemma 3.1 *Let* $\mathbf{V}$ *be a linear space,* $\mathcal{H} : \mathbf{V} \to \mathbf{R}$ *be convex and differentiable*[2]*,* $\mathcal{I} : \mathbf{V} \to \mathbf{R}$ *be convex and* $\mathcal{J} = \mathcal{H} + \mathcal{I}$*. Then for all* $\mathbf{v} \in \mathbf{V}$ *it holds*

$$\mathcal{J}(\mathbf{v}) \le \mathcal{J}(\mathbf{w}) \quad \forall w \in \mathbf{V} \quad \Leftrightarrow \quad (\mathcal{H}'(\mathbf{v}),\mathbf{w}-\mathbf{v}) + \mathcal{I}(\mathbf{w}) - \mathcal{I}(\mathbf{v}) \ge 0 \quad \forall w \in \mathbf{V}.$$

Proof:

(i) $\mathcal{H}$ convex immediately implies $(\mathcal{H}'(\mathbf{v}),\mathbf{w}-\mathbf{v}) \le \mathcal{H}(\mathbf{w}) - \mathcal{H}(\mathbf{v})$, so that $\mathcal{J}(\mathbf{v}) \le \mathcal{J}(\mathbf{w})$.

(ii) The proof of the reverse implication uses the convexity of $\mathcal{I}$.

$$\begin{aligned}
&(\mathcal{H}'(\mathbf{v}),\mathbf{w}-\mathbf{v}) + \mathcal{I}(\mathbf{w}) - \mathcal{I}(\mathbf{v}) = \\
&\quad = \lim_{t\to 0+} \frac{1}{t}(\mathcal{H}(\mathbf{v}+t(\mathbf{w}-\mathbf{v})) - \mathcal{H}(\mathbf{v}) + t(\mathcal{I}(\mathbf{w}) - \mathcal{I}(\mathbf{v}))) \ge \\
&\quad \ge \lim_{t\to 0+} \frac{1}{t}(\mathcal{H}(\mathbf{v}+t(\mathbf{w}-\mathbf{v})) - \mathcal{H}(\mathbf{v}) + \mathcal{I}(\mathbf{v}+t(\mathbf{w}-\mathbf{v})) - \mathcal{I}(\mathbf{v})) = \\
&\quad = \lim_{t\to 0+} \frac{1}{t}(\mathcal{J}(\mathbf{v}+t(\mathbf{w}-\mathbf{v})) - \mathcal{J}(\mathbf{v})) \ge 0.
\end{aligned}$$

□

The analysis of the problem can be found in [3].

4 Numerical results

The obtained results are based on the bilateral contact problem with or without friction in elasticity and the finite element method. The model problem is formulated as primary contact problem (i.e. in displacements), where the geometry of the weight-bearing tibia is based on its cross-section in the sagittal plane (see Fig.1). The investigated tibial area in the sagittal plane occupies the region, we denote it by Ω as above in Section 2.1 and its boundary by $\partial\Omega = \Gamma_D \cup \Gamma_L \cup \Gamma_C$. The boundary $\partial\Omega$ is created by the part Γ_D, where the tibia is fixed (in the figure demonstrated by the red line), by the part ${}^1\Gamma_L$, where the loads are prescribed (which in the figure are demonstrated by the green

[2] i.e. there exists $\lim_{t\to 0+} \frac{1}{t}(\mathbf{H}(\mathbf{v}+t\mathbf{w}) - \mathbf{H}(\mathbf{v}))$ for all $\mathbf{v},\mathbf{w} \in \mathbf{V}$.

arrows) and by ${}^2\Gamma_L$, where the surface of tibia is unloaded, and by the part, we denote it by Γ_C, the contact surface between the bone and the marrow. On the boundary Γ_C the bilateral contact boundary conditions are prescribed.

Discussion of numerical results

The numerical results are presented in Figs 1-9. The geometry of the weight-bearing tibia is given in Fig.1. The magnitude of the loading is $2.0 \times 10^6 Pa$. In Fig.1 the bone tissue is colored dark brown, while the marrow is colored light brown. Table 1 summarizes the biomaterial constants used in the

Material	**Elastic modulus** [Pa]	**Poisson's ratio** [1]
Bone tissue	1.71×10^{10}	0.25
Marrow	2.0×10^6	0.49

Table 1: Material constants

computation. The articular cartilage is not assumed in the investigated model. Deformation of the long bone, the tibia, is presented in Fig.2. Small bending of the tibia in its middle part is observed. In Figs 3 and 4 the horizontal and vertical components of displacement vector are presented. The horizontal component of displacement vector indicates the bending in the middle part of tibia, while the vertical component of displacement vector indicates certain vertical displacement changes in the marrow, namely in the middle part of tibia. Moreover, it indicates elementary shifts of the biomaterial points of the marrow tissue on the contact surface between the bone tissue and the marrow, as well as elementary shifts in the marrow tissue inside the tubular bone. Figs 5-7 represent distributions of the horizontal, vertical and shear stresses. Numerical results show that greater changes of horizontal stresses are observed in the areas near the points 2 and 3 and on both sides of the point 1 in the epiphyses and smaller changes also in the bone tissue. The vertical stresses indicate changes in pressures on the outside right part of bone tissue in the middle tibia and on the inside left part of the middle tibia tissue, while changes in tensile stresses are observed in the inside right part of the bone tissue and in the outside left part of the middle tibia tissue. Moreover, it also indicates the probability of small changes in vertical stresses in the marrow area. Changes of shear stresses are observed in the middle part of tibia and in the areas between the marrow and bone tissues in the epiphyses. Greater changes of shear stresses can be also observed in the epiphyses of tibia. The elementary changes of tangential stresses on the contact surface between the marrow and the bone tissues are also indicated. The principal stresses in Fig.8 and Fig.9 show that the great value of loading is transported through the bone tissue as the compression in the predominance on the right outer part of the compact bone and through the layer of small thickness near the left inside wall of the bone, while the outer left part of the bone tissue in the middle tibia is characterized by the tensile stresses. Moreover, the compression is also observed in the spongy bone of both epiphyses. The principal stresses presented in Fig.8 show that the great loading is transported through the right side of tubular tibia. On the contact boundary between the bone and the marrow tissues small tangential shifts can be expected. All these observed effects are consequences of bending in the middle part of tibia. Furthermore, we see that Figures 5-8 show that a great value of loading is transported through the bone tissue. In Fig.9 the distribution of principle stresses in the medullar cavity filled by the yellow marrow is presented in details. We see that the yellow marrow in the medullar cavity in its upper and lower parts are compressed, and that the magnitude of stresses in both areas are 1000-times lower than in the corticalis of tubular tibia, while the distribution of stress field in the yellow marrow in the middle part of tubular tibia in the consequence of bending is characterized by greater area of tensions, the magnitude of which is of about several orders lower than tensions or compressions in the bone tissue and of one order lower than compressions in the marrow of the upper and lower parts of medullar cavity. In the figures the blue arrows refer to tensile stresses while the red arrows refer to the pressures.

5 Conclusion

From the above analyses of the weight-bearing tubular tibia we see that a great value of loading is transported through the bone tissue, and moreover, that small bending of the tibia in its middle part

is observed. Numerical results indicate that the yellow marrow in the medullar cavity in its upper and lower parts are compressed, and that the magnitude of stresses in both areas are 1000-times lower than in the corticalis of tubular tibia, and moreover, that the distribution of stress field in the yellow marrow in the middle part of tubular tibia, in the consequence of bending, is characterized by a greater area of tensions with the magnitude which is of about several orders lower than tensions or compressions in the bone tissue and of one order lower than compressions in the marrow of the upper and lower parts of medullar cavity. Convincing biomechanical analyses can give the analyses of the TKR (and or the artificial replacements of hip joint) models, which will analyse distributions of stresses in areas near the tibial stem of the artificial knee joint.

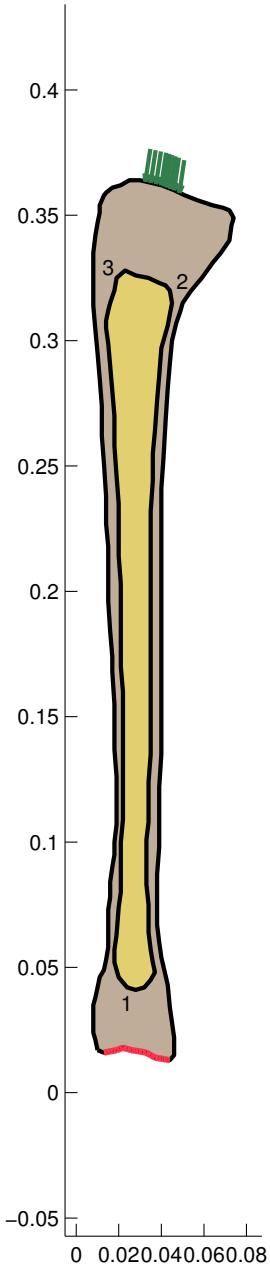

Figure 1: Geometrical settings

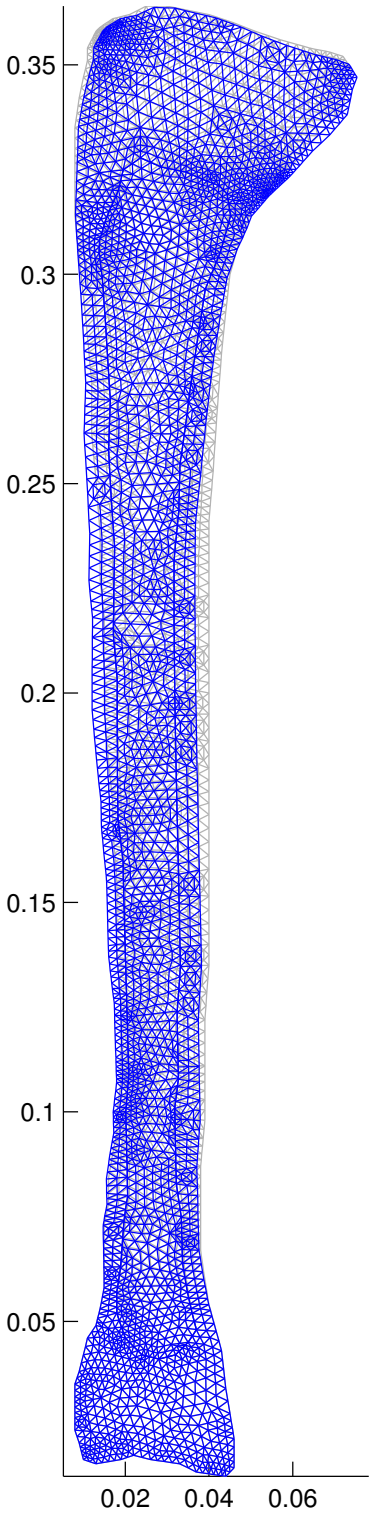

Figure 2: The Deformation

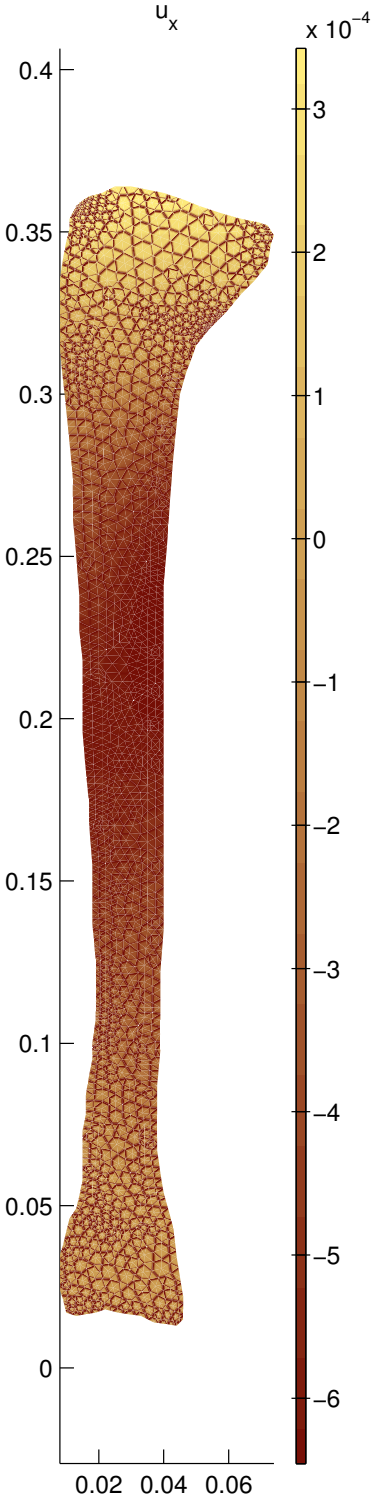

Figure 3: Horizontal Displacement

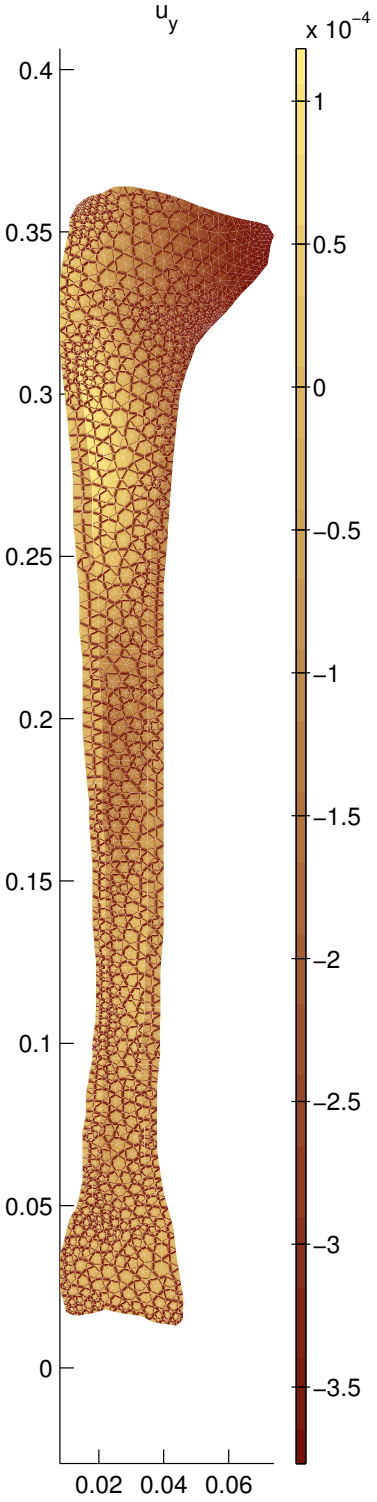

Figure 4: Vertical Displacement

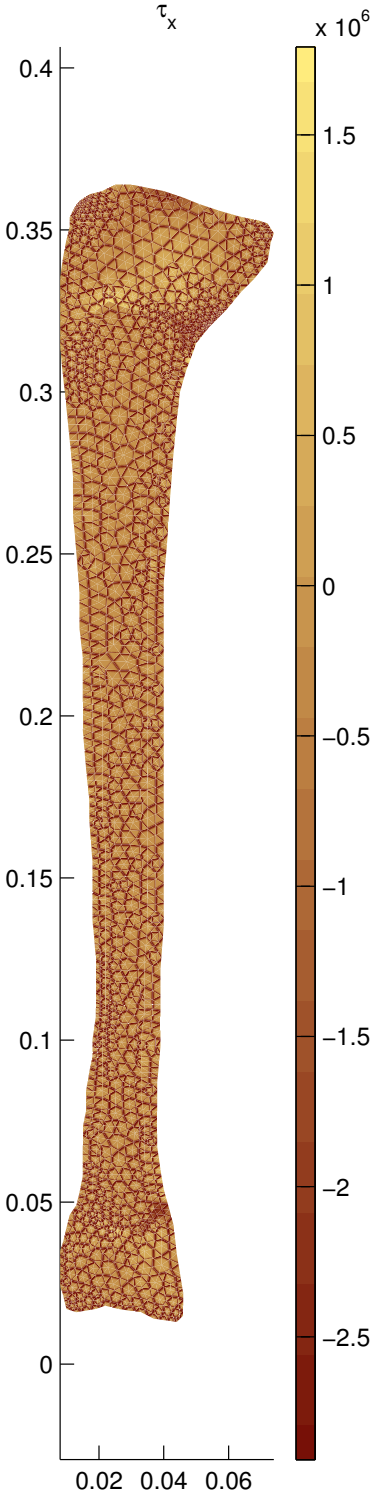

Figure 5: Horizontal Stress

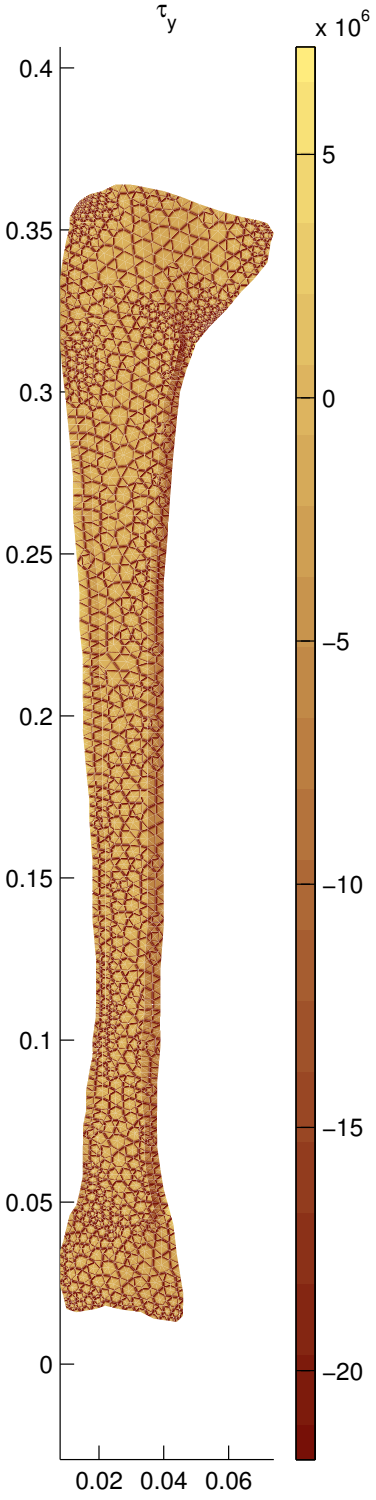

Figure 6: Vertical Stress

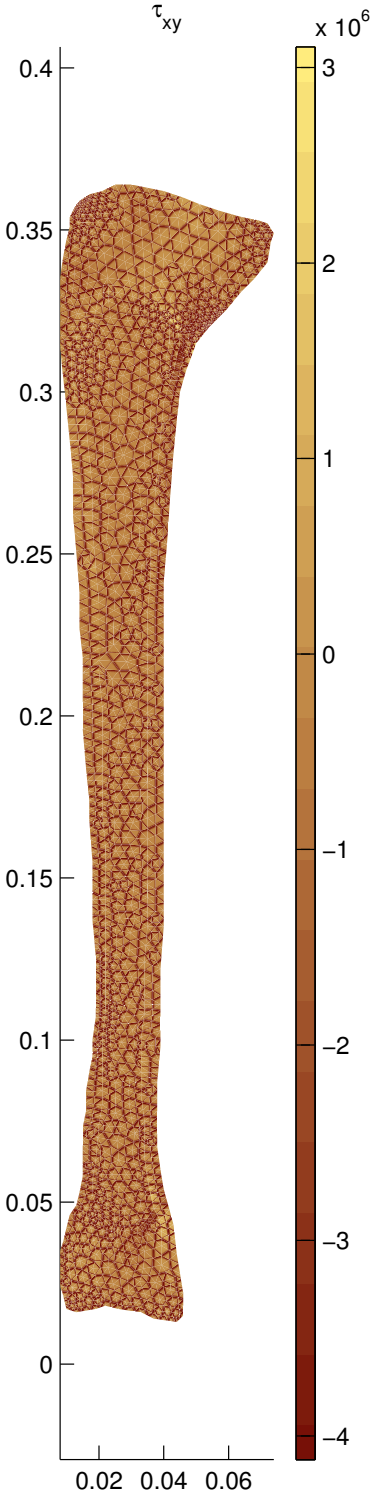

Figure 7: Shear Stress

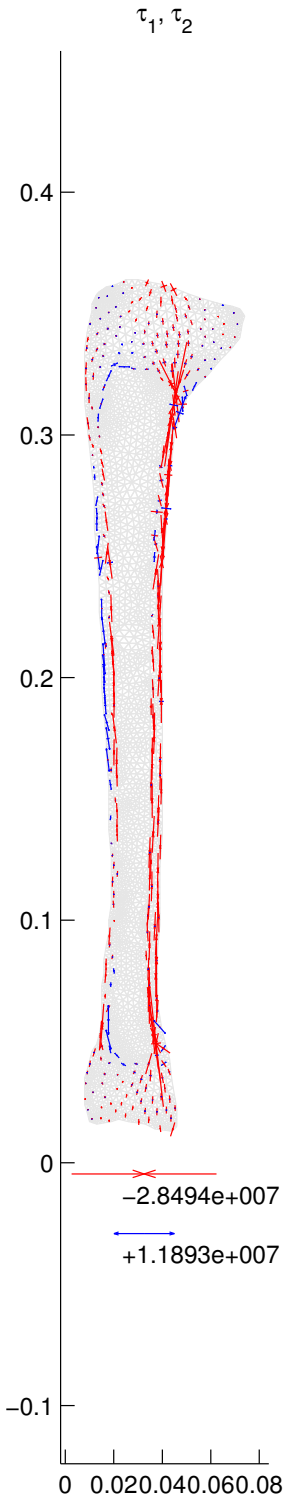

Figure 8: Principle Stress

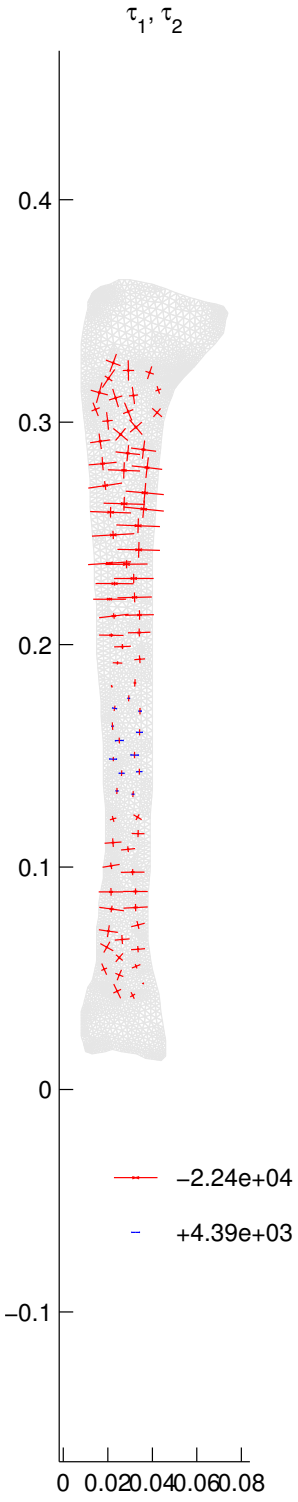

Figure 9: Principle Stress - Detail

Bibliography

[1] Daněk J.: Výsledky numerického modelování zatížené keramické náhrady kolenního kloubu, Tech. Rep. V-990, ICS AS CR, Prague, 2007.

[2] Daněk J., Stehlík J., Nedoma J., Hlaváček I.: Výsledky numerického modelování zatíženého kolenního kloubu a jeho náhrady s uvažováním kloubního pouzdra, Tech. Rep. V-983, ICS AS CR, Prague, 2006.

[3] Duvaut G. , Lions J.L.: Inequalities in Mechanics and Physics. Springer Vlg., Berlin, Heidelberg, New York, 1976.

[4] Nedoma J., Tomášek L.: Zatížení trubkovité kosti vyplněné kostní dření: numerické řešení 2D modelové úlohy, Tech. Rep. V-984, ICS AS CR, Prague, 2006.

[5] Roubíček T.: Nonlinear Partial Differential Equations with Applications, Birkhäuser, Basel, 2005.